



Aqueous-phase hydrodeoxygenation of carboxylic acids to alcohols or alkanes over supported Ru catalysts

Lungang Chen^{a,b}, Yulei Zhu^{a,c,*}, Hongyan Zheng^c, Chenghua Zhang^{a,c}, Bin Zhang^{a,b}, Yongwang Li^{a,c}

^a State Key Laboratory of Coal Conversion, Institute of Coal Chemistry, Chinese Academy of Sciences, P.O. Box 165, Taiyuan 030001, PR China

^b Graduate University of the Chinese Academy of Sciences, Beijing 100039, PR China

^c Synfuels China Co. Ltd., Taiyuan 030032, PR China

ARTICLE INFO

Article history:

Received 2 August 2011

Received in revised form 12 October 2011

Accepted 14 October 2011

Available online 20 October 2011

Keywords:

Hydrodeoxygenation

Ru

Carboxylic acid

C–C cleavage

Decarbonylation

ABSTRACT

For the aqueous-phase hydrodeoxygenation (APHDO) of carboxylic acids over the Ru/C, Ru/ZrO₂ and Ru/Al₂O₃ catalysts, the C=O hydrogenation and C–C bond cleavage reactions were studied by collecting reaction kinetics data and the measures of DRIFTS. The C–C bond cleavage was improved at high temperature and with high metal loadings. The acidic supports in combination with Ru metal can favor the C=O hydrogenation of carboxyl. The C–C bond cleavage derived from the decarbonylation of acyl on the catalyst was studied by the measures of DRIFTS. The APHDO and DRIFTS results demonstrated that the C–C bond cleavage was favored in the order of Ru/C > Ru/ZrO₂ > Ru/Al₂O₃. The catalysts were characterized by multiple methods (H₂-TPR, NH₃-TPD, CO-FTIR and DRIFTS of propanoic acid). It is concluded that the effect of support on the reaction routes may be attributed to these factors of catalysts, i.e., surface acidity, metal–support interaction and electronic state of Ru species.

© 2011 Elsevier B.V. All rights reserved.

1. Introduction

Biomass is a promising candidate to serve as a sustainable source of organic carbon for the production of industrial chemicals [1]. The available strategies for transforming biomass to bio-fuels and/or chemicals have been attracted more interestingly. In future, the range of block chemicals from biorefineries is extensive and is expected to become greater with further research [2–5]. Generally, these block chemicals, i.e., the so-called platform molecules, are defined as chemicals containing multiple functional groups (e.g., acids, ketones, alcohols, amines, etc.). It is imperative to develop more efficient processes for catalytic upgrading of these block chemicals. However, lots of potential feedstocks are produced along with water from biomass by fermentation and/or hydrolysis routes [4]. However, removal of water from these compositions would be time-consuming and costly, and water has many advantages over more conventional solvents that present problems with toxicity and difficulties with handling and disposal. Considering these factors, the aqueous-phase hydrodeoxygenation (APHDO) reactions [6–21] are a crucial component of a number of strategies for the conversion of biomass-derived feedstocks into fuels and chem-

icals, e.g., hydrogenation of targeted functionalities of biomass including acids, sugars, aldehydes and furans. Many groups have extensively worked on these (e.g., Dumesic [8–11,15,20,22], Miller and Jackson groups [6,7,12,13,23], Huber [17,20,22,24–28], Corma [29], Clark and Luque groups [30,31]), including alcohol production from organic acids [6,12,17,23], gasoline production from bio-oils [28], and alkane production from carbohydrates [8,11,20,22].

The APHDO of carboxylic acids to alcohols has been investigated as a possible pathway for production of novel, high-valued products from bio-derived feedstock [23]. The direct APHDO of organic acids offers an alternative that is atom economical and amenable to continuous processing, and that obviates the need for intermediate esterification, use of organic solvents, and byproduct waste streams [23]. Recently, Miller and Jackson groups have studied the APHDO of propanoic acid and lactic acid over the Ru/C catalyst [6,12,13]. They demonstrated that production of alcohol was improved at lower temperature and higher hydrogen pressures, and the methane, ethane and propane were detected as the main by-products. In addition, many degraded alkane byproducts were produced in the hydrogenolysis of glycerol to propylene glycol over the Ru-base catalysts [32–35]. In these reactions, the cleavage of C–C bonds and the formation of methane were proposed to occur primarily through a metal-catalyzed reaction on Ru [33]. Thus, selectively removing oxygen from the biomass-derived compounds is one of the key challenges in converting renewable biomass resources into fuels and chemicals. The oxygen is removed from the biomass with the APHDO by a combination of the C=O hydrogenation, the C–O

* Corresponding author at: State Key Laboratory of Coal Conversion, Institute of Coal Chemistry, Chinese Academy of Sciences, P.O. Box 165, Taiyuan 030001, PR China. Tel.: +86 351 7117097; fax: +86 351 7560668.

E-mail address: zhuyulei@sxicc.ac.cn (Y. Zhu).

bond cleavage and the C–C bond cleavage reactions. If the larger alkanes or upgraded oxygenates are desired, then the C–C bond cleavage should be inhibited and the C=O hydrogenation and the C–O bond cleavage should be strengthened. If the degraded alkanes are desired, then the C–C bond cleavage should be enhanced. Therefore, it is necessary to understand the C=O hydrogenation and C–C bond cleavage reactions over the supported Ru catalysts, since the ruthenium is a promising catalyst for the conversion of biomass feedstock to various chemicals [6,12,13,31–37].

In this work, the APHDO of carboxylic acids (C₂–C₄), especially propanoic acid served as a probe molecule, was studied to understand the catalytic performance of several supported Ru catalysts (Ru/C, Ru/ZrO₂ and Ru/Al₂O₃). The goal was to identify key reaction intermediate and to reveal the reaction mechanisms of the C=O hydrogenation and C–C bond cleavage on supported Ru catalysts. The different reaction routes (C=O hydrogenation of carboxyl and C–C bond cleavage) were investigated in detail. In particular, the DRIFTS of propanoic acid were performed to understand the mechanism of the C–C bond cleavage. The effect of support on the hydrodeoxygenation routes was discussed based on the characterizations of catalysts (H₂-TPR, NH₃-TPD, CO-FTIR and DRIFTS of propanoic acid). In the present contribution, the APHDO reaction can be tuned to make a targeted product (alkanes or upgraded oxygenates) from biomass-derived chemicals by the improvement in the catalyst design.

2. Experimental

2.1. Catalyst preparation

Supported Ru catalysts were prepared by incipient wetness impregnation with an aqueous solution containing corresponding metal precursors (RuCl₃·3H₂O, Shaaxi Kaida Chemical Engineering Co., Ltd., China) at ambient for 12 h, followed by drying at 120 °C for 12 h. Subsequently, the catalysts were calcined at 500 °C in air for 6 h except the Ru/C catalyst. Prior to impregnation, the supports ZrO₂ (S_{BET} = 58 m² g⁻¹, Jiangsu Qianye Co., Ltd., China), γ-Al₂O₃ (S_{BET} = 197 m² g⁻¹, Shandong Aluminum Co., Ltd., China) and granular coconut carbon (referred to as C, S_{BET} = 1091 m² g⁻¹, Liyang Zhuxi Carbon Co., Ltd., China) were soaked in deionized water for 24 h at ambient, and then dried at 120 °C. The catalysts are generally labeled as (n)metal/support, in which the number *n* represents nominal metal loading, e.g., the 1.0Ru/ZrO₂ stands for a Ru metal supported on the ZrO₂ support with 1.0 wt% metal loading.

2.2. Catalyst characterizations

N₂-physisorption was carried out at –196 °C in a Micromeritics ASAP 2420 (USA) instrument. Before the measurements, the samples were first outgassed overnight at 250 °C to 50 mTorr. The specific surface area was estimated by the BET (Brunauer–Emmett–Teller) method.

Metal dispersion was determined by CO and H₂ pulse chemisorption performed in a Micromeritics Auto Chem. 2920 (USA) apparatus with a thermal conductivity detector (TCD). The pre-treatment of catalyst was performed in the H₂ flow at 300 °C for 2 h, followed by degassing in flowing Ar at 350 °C. Pulse chemisorption was carried out at 0 °C. Several pulses of H₂ (or CO) were injected at regular intervals, until the area of the recorded peaks became constant. Dispersion values were calculated from quantification of the chemisorbed H₂ (or CO) based on the assumption that the stoichiometry factor of chemisorbed H₂ (or CO) to surface Ru equals H (CO)/Ru = 1.

The acidic property of the catalyst was studied by ammonia temperature-programmed desorption (NH₃-TPD). The NH₃-TPD was measured by the same apparatus with chemisorption. The catalysts (100 mg) were pretreated in flowing H₂ at 300 °C for 2 h, followed by degassing in flowing He at 350 °C and then cooled to 100 °C under a 50 cm³ min⁻¹ He flow. The pretreated samples were saturated with NH₃ for 1 h at 100 °C, with subsequent flushing with helium at 100 °C for 2 h to remove the physisorbed NH₃. Finally, the sample was heated from 100 °C up to 800 °C at a rate of 10 °C min⁻¹.

The temperature-programmed reduction by H₂ (H₂-TPR) was performed in the same apparatus with chemisorption. When needed, a quadrupole mass spectrometer (MS) was connected with the TPR system for the detailed analysis of the outlet gas. The samples (100 mg) were dried under Argon flow at 150 °C for 60 min, and then cooled to 40 °C. Then, the Argon flow was switched to 10 vol% H₂/Ar mixed gas, and a cold trap with isopropanol–liquid nitrogen slurry was added to condense the water vapor. After the TCD signal returned to the baseline, the reduction was carried out from 40 °C up to 800 °C with a ramp of 10 °C min⁻¹.

CO-FTIR spectra were recorded by an infrared spectrometer (VERTEX70, Bruker, Germany), equipped with KBr optics which works at the liquid nitrogen temperature. The infrared cell with ZnSe windows was connected to a gas-feed system with a set of stainless steel gas lines, which allowed the in situ measurement for the adsorption of CO. Before measurements, the catalysts were reduced in situ at 300 °C for 2 h. After the reduction procedure, the system was cooled to 20 °C. The CO-FTIR spectra were recorded following adsorption of CO at 20 °C, subsequently, desorption of CO in He at the higher temperature (50–170 °C).

The propanoic acid chemisorption on the catalyst surface was performed by in situ diffuse reflectance infrared transform spectra (DRIFTS) measurement using a VERTEX70 spectrometer cooled by liquid nitrogen. A vacuum pump was used to pull the propanoic acid vapor through the chamber for in situ DRIFTS measurements. Before the measurements, the catalysts were reduced in situ at 300 °C for 3 h. After the reduction procedure, the system was cooled to 180 °C and the DRIFTS spectra of propanoic acid were recorded. Then, the temperature was increased from 180 °C to 210 or 270 °C under flowing H₂. For the DRIFTS spectra of propanoic acid adsorption on catalysts in the absence of H₂, the system was cooled to 50 °C after the reduction of catalysts, and then the DRIFTS spectra were recorded at 50 °C, subsequently, recorded with TPD (50–400 °C). The spectra were recorded with a cumulative averaging of 64 scans and at a resolution of 4 cm⁻¹.

2.3. Catalytic test

Experimental studies were carried out using a continuous-flow trickle-bed reactor (i.d. 11 mm and length 1300 mm), in which 6.0 g of catalyst was packed. Before the reactions, the catalysts were first activated by in situ reduced in a H₂ flow of 80 cm³ min⁻¹ at 300 °C for 3 h. To ensure an aqueous-phase system, the APHDO of carboxylic acids was operated at 6.4 MPa total pressures. The feedstock was introduced into the reactor with an HPLC pump along with a co-feed H₂ of gas flowing at 80 cm³ min⁻¹. The effluent aqueous phase was collected in a gas–liquid separator immersed in ice–water. The products were obtained when the reaction reached the steady state. The mass balance closure in every experiment was achieved within 5% deviation from the inlet feedstock.

The aqueous phase products in the ice trap were analyzed off-line by an Agilent 6980 gas chromatography (GC) equipped with a FID detector and a DB-WAX (30 m × 0.32 mm) capillary column. The concentrations of H₂, CO and CO₂ were determined on-line by an Agilent 7980 GC equipped with a Porapak Q stainless steel packed column, a PLOT Q packed column, a molecular sieve (5A) packed column, and a TCD detector. The gaseous alkanes were analyzed

Table 1
Physicochemical properties and surface acidity of the supported Ru catalysts.

Catalyst	S_{BET} ($\text{m}^2 \text{g}^{-1}$)	Dispersion (%) ^a		Acid sites ($\mu\text{mol NH}_3 \text{m}^{-2}$) ^b			Total
		H ₂	CO	Weak <250 °C	Medium 250–400 °C	Strong >400 °C	
1.0Ru/C	1021	30.2	88.1	0.3	0	0	0.3
1.0Ru/ZrO ₂	52	12.7	36.7	9.6	34.6	0	44.2
1.0Ru/Al ₂ O ₃	185	4.4	7.1	38.4	57.8	11.9	108

^a The metal dispersion was measured by H₂ and CO pulse chemisorption at 0 °C.

^b Amount of desorbed ammonia was determined by NH₃-TPD.

on-line by an Agilent 7980 GC equipped with a FID detector and an Al₂O₃ capillary column. The conversion and the selectivity of products in the present study were calculated based on the following equations:

$$\text{Conversion (\%)} = 100 - \frac{\text{Carbon mol of reactants after reaction}}{\text{Carbon mol of reactants in feedstock}} \times 100$$

$$\text{Selectivity (\%)} = \frac{\text{Carbon mol of each product in gas or aqueous phase}}{\text{Sum of carbon mol for all products}} \times 100$$

3. Results and discussion

3.1. Catalyst characterizations

3.1.1. BET surface area and pulse chemisorption of H₂ and CO

BET surface area and Ru dispersion of catalysts are shown in Table 1. The Ru/ZrO₂ catalyst has a small BET surface area of 52 m² g⁻¹ compared with the Ru/C (1021 m² g⁻¹) and Ru/Al₂O₃ (185 m² g⁻¹) catalysts. The Ru dispersion determined by H₂ or CO pulse chemisorption increases in the same order: Ru/Al₂O₃ < Ru/ZrO₂ < Ru/C. Nevertheless, the Ru dispersion measured by H₂ pulse chemisorption is lower than that determined by CO pulse chemisorption. This behavior may result from the strongly corrosive chemisorption and/or multiple adsorption of CO on the supported Ru catalysts [38].

3.1.2. Surface acidity of catalysts

The ammonia desorption curves and the acidity values of catalysts (expressed as the amount of desorbed ammonia per unit surface area of catalyst, $\mu\text{mol NH}_3 \text{m}^{-2}$) are compiled in Fig. 1 and Table 1, respectively. The density of acid sites on the catalyst surface increases in the following order: Ru/C < Ru/ZrO₂ < Ru/Al₂O₃ (Table 1). As shown in Fig. 1, just one weak peak appears at 190 °C in the profile of Ru/C, and no peak is observed obviously above

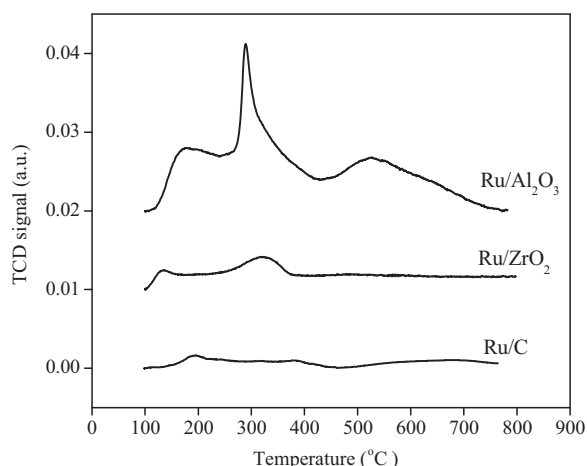


Fig. 1. NH₃-TPD profiles of the supported Ru catalysts.

300 °C. In case of Ru/ZrO₂, two main peaks appear in the temperature range of 100–200 °C and 200–400 °C, indicating the presence of weak and medium acid sites. The Ru/Al₂O₃ catalyst has three peaks corresponding to weak, medium and strong acid sites, respectively.

3.1.3. Temperature programmed reduction of H₂

Fig. 2 illustrates the H₂-TPR profiles for the unsupported bulk RuO₂ and the supported Ru catalysts. The unsupported RuO₂ shows a highly sharp peak at 102 °C. The amount of H₂ consumed in the reduction of RuO₂ is calculated, which is almost comparable with the theoretical value (198 $\mu\text{mol g}^{-1}$) calculated by assuming the reduction of RuO₂ to Ru. In fact, Hosokawa et al. [39] have reported that Ru ion in RuO₂ changes directly from Ru⁴⁺ to Ru⁰ without forming intermediate valence states such as Ru³⁺ or Ru²⁺. Thus, the H₂ consumption in TPR runs can be ascribed to the reduction of RuO₂ to Ru metal.

For the supported Ru catalysts, the reduction temperature is strongly dependent on the nature of support. The reduction peaks are observed at around 85 °C and 150–300 °C for the Ru/C catalyst. The temperature of first peak is lower than that of unsupported RuO₂, indicating that this peak is due to reduction of well dispersed RuO₂ on the active carbon surface [40,41]. Besides, the MS analysis confirms that CH₄ formation connects with the peak above 150 °C. It can be concluded that the supported Ru particles catalyze the breaking of the weakest C–C bonds on the surface of active carbon [42]. The efficiency of this catalytic action improves greatly at the higher temperature, and it is indicated by the uphill of the TCD signal in the TPR of Ru/C catalyst (Fig. 2). In the case of Ru/ZrO₂, two reduction peaks are observed at around 90 °C and 132 °C, which are in agreement with the previous report [43]. Furthermore, a broad peak appears at around 430 °C is due to the promoted support reduction through spillover of hydrogen species from Ru onto ZrO₂

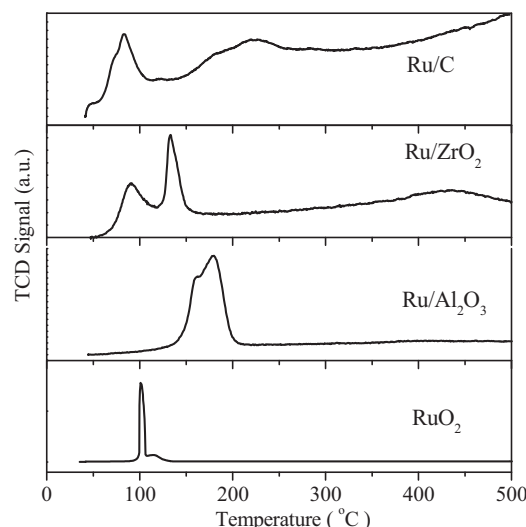


Fig. 2. H₂-TPR profiles of the supported Ru catalysts.

[44]. For the Ru/Al₂O₃ catalyst, two overlapped H₂ consumption peaks occur at relatively higher temperature of 120–200 °C than that of bulk RuO₂ (102 °C). It is usually accepted that the reduction of RuO₂ to Ru at lower temperature is attributed to highly dispersed RuO₂ species, while at higher temperature is attributed to the reduction of well crystallized RuO₂ particles [40,41]. For the Ru/C and Ru/ZrO₂ catalysts, the low temperature peaks in the TPR are dominant, while the high temperature peaks are great for the Ru/Al₂O₃ catalyst. These indicate that the well-dispersed Ru particles on the Ru/C and Ru/ZrO₂ catalysts are greater than those of Ru/Al₂O₃ catalyst. However, the metal-support interaction of catalyst can greatly influence the reducibility of the Ru species. For all catalysts, the maximal reduction temperature increases in the following order: Ru/C < Ru/ZrO₂ < Ru/Al₂O₃, indicating that the support material greatly influences the reducibility of the Ru species. Indeed, the strong metal–support interaction (SMSI) is the reason of the increased reduction temperature of the ruthenium species on Al₂O₃ compared with ZrO₂ [45]. Asakura and Iwasawa [46] have reported that the Ru species on Al₂O₃ have strong chemical interaction between metal and support through the Ru–O–Al bonding by extended X-ray absorption fine-structure (EXAFS) analysis. They suggested that the interaction between metal and support could be explained by the electronegativities of support metal ions.

3.1.4. CO-FTIR

FTIR spectroscopy of adsorbed CO is a method for the characterization of the electronic states of supported metals. Several FTIR studies have been conducted with Ru catalysts employing the probe molecule CO [47–49], where the ability of adsorbed carbon monoxide to respond sensitively to the environment of the adsorbing metal atoms is utilized to indicate the electronic state of the adsorption site by the C–O vibration frequency. Generally, CO linearly bonded on Ru⁰ produces a low frequency (LF) absorption bands in the 1990–2060 cm⁻¹ region [49,50]. High frequency (HF) bands in around 2060–2156 cm⁻¹ region are attributed to the multicarbonyl species adsorbed on partially oxidized Ru sites [49–51]. These Ru sites are mostly produced by the oxidative disruption of very small Ru clusters with the participation of hydroxyl groups of the support [49,50].

The FTIR spectra of CO adsorbed on the 1.0Ru/ZrO₂ and 1.0Ru/Al₂O₃ samples are displayed in Fig. 3. In the case of Ru/ZrO₂ catalyst (Fig. 3a), the 2033 cm⁻¹ band disappears at 80 °C with increasing temperature, and the band located at 2135 cm⁻¹ decreases without exhibiting any frequency shift and disappears at 170 °C. At the same time, the 2002 cm⁻¹ band appears at 50 °C and becomes clear with a red shift from 2003 to 1996 cm⁻¹ with the temperature increasing from 50 to 170 °C. The intensity of 2066 and 2002 cm⁻¹ bands decrease obviously from 50 to 110 °C, but they can still exhibit high intensity at the higher temperatures. In the case of Ru/Al₂O₃ catalyst (Fig. 3b), adsorption of CO at 20 °C produces three IR features at 2125, 2068 and 2025 cm⁻¹. The band located at 2025 cm⁻¹ exhibits a little shift to 2015 cm⁻¹ at 110 °C and disappears at above 140 °C with the increase of temperature. The intensity of 2068 cm⁻¹ band decreases and even disappears with the temperature increasing from 20 to 110 °C. Subsequently, the 2051 cm⁻¹ appears at 140 °C and its intensity increases with temperature increasing to 170 °C. Meanwhile, the 2125 cm⁻¹ band follows the same trend of disappearance/appearance at between 110 and 140 °C and then becomes stronger and broader with temperature increasing. Fig. 3a and b demonstrate that the thermal stability of the CO species adsorbed on Ru/ZrO₂ catalyst is different from that of Ru/Al₂O₃ catalyst. The 2002 and 2066 cm⁻¹ bands are more stable over the Ru/ZrO₂ catalyst than that the 2025 and 2068 cm⁻¹ bands over the Ru/Al₂O₃ catalyst. The frequency of LF band on the Ru/ZrO₂ catalyst (2002 cm⁻¹) is lower than that of the Ru/Al₂O₃ catalyst (2025 cm⁻¹). This may indicate

that the electronic state of Ru species is different between the Ru/ZrO₂ and Ru/Al₂O₃ catalysts. In addition, a particular interest is that the 2051 and 2125 cm⁻¹ bands follow the trend of disappearance/appearance upon thermal desorption over the Ru/Al₂O₃ catalyst, while this trend is not observed on the Ru/ZrO₂ catalyst. Generally, these HF bands are attributed to multicarbonyl species adsorbed on oxidized Ru sites [49–51]. Indeed, Chin et al. [49] have demonstrated that a significant part of Ru species exists in its oxidized form on the Ru/Al₂O₃ catalyst by X-ray photoelectron spectroscopy (XPS) and CO-FTIR techniques. The current CO-FTIR study shows that the Ru/Al₂O₃ catalyst exhibits relatively unstable adsorption of CO species and reappearance of multicarbonyl species at the high temperatures compared with the Ru/ZrO₂ catalyst. It is possible that the Ru metal over the Ru/Al₂O₃ catalyst is more easily reoxidated and is more unstabilized at the high temperature than that over the Ru/ZrO₂ catalyst, which may be attributed to the nature of support and the redox behavior of the dispersed metal [51]. Furthermore, Mazzieri et al. [52] have reported that the HF bands characterize electron deficient ruthenium species (Ruⁿ⁺) in different oxidation states. They have confirmed that the electron deficient species are the origin of the HF bands by X-ray photoelectron spectroscopy (XPS) technique. Mitsui et al. [53] have analyzed the electronic state of supported Ru catalysts by XPS. They have reported that the binding energy of reduced Ru/Al₂O₃ catalyst (280.8 eV) is higher than that of reduced Ru/ZrO₂ catalyst (279.8 eV). Therefore, it is speculated that the electron deficient ruthenium species (Ruⁿ⁺) on the Ru/Al₂O₃ catalyst are more than those on the Ru/ZrO₂ catalyst.

3.2. DRIFTS of propanoic acid over the Ru/ZrO₂ and Ru/Al₂O₃ catalysts

In order to obtain the information about the adsorbed intermediates on catalyst surface, the DRIFTS of propanoic acid adsorbed on the catalysts were performed. In the case of Ru/ZrO₂ catalyst, Fig. 4a illustrates that the two bands at 1303 and 1382 cm⁻¹ may be ascribed to $\delta_s(-CH_3)$ and $\delta_{as}(-CH_3)$ [54–57], and the three weak bands at 2886, 2950, and 2983 cm⁻¹ are ascribed to the C–H stretching in $\nu_{as}(-CH_3)$, $\nu_{as}(-CH_2)$ and $\nu_s(-CH_3)$ [55,56,58], respectively. At 50 °C, a broad band at 1521 cm⁻¹ and a very weak shoulder band at 1475 cm⁻¹ are ascribed to asymmetric $\nu_{as}(-COO)$ and symmetric $\nu_s(-COO)$ stretching of adsorbed propionate species [55,56], respectively. As temperature increases from 50 to 400 °C, the 1475 cm⁻¹ band appears and its intensity becomes very weak at 400 °C. The 1303, 1382 and 1521 cm⁻¹ bands don't exhibit any frequency shift but change of intensity. However, the $\nu(-CO)$ stretching of propanoyl species shifts from 1682 to 1621 cm⁻¹ [55,56,59] and the intensity of band becomes very weak at 400 °C. At the same time, the bands of adsorbed CO at 1868, 1987 and 2065 cm⁻¹ [49–51], as well as, the bands of adsorbed CO₂ at 2335 and 2362 cm⁻¹ [60] appear above 200 °C. Based on this information, it is speculative that the configuration of adsorbed propanoyl species is transformed to another configuration which is easily dissociated to CO through decarbonylation with the increase of temperature. However, the decomposition of propionate to CO/CO₂ cannot be excluded at the high temperature. For the Ru/Al₂O₃ catalyst (Fig. 4b), in the same way, the bands of $\delta(-CH_3)$ (1308 and 1370 cm⁻¹), $\nu(-CH_3)$ (2889, 2946 and 2981 cm⁻¹), $\nu(-COO)$ of propionate (1503 and 1538 cm⁻¹), and $\nu(-CO)$ stretching of propanoyl (1707 cm⁻¹) were observed at 50 °C. The intensity of these bands decreases greatly without exhibiting any obvious frequency shift with the increasing of temperature, just the 1707 cm⁻¹ band ($\nu(-CO)$ stretching of propanoyl) exhibits a little red shift to 1692 cm⁻¹. However, the bands of adsorbed CO and CO₂ appear very weakly even at the higher temperatures. These results display that the propionate and propanoyl species on the Ru/Al₂O₃

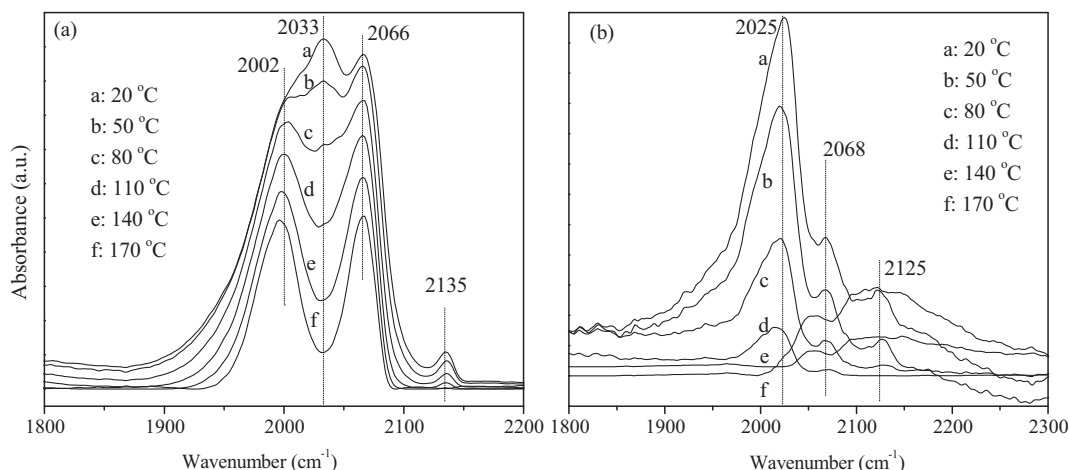


Fig. 3. FTIR spectra of CO adsorbed at 20 °C over the 1.0Ru/ZrO₂ (a) and 1.0Ru/Al₂O₃ (b) catalysts, then desorbed in the range of 50–170 °C.

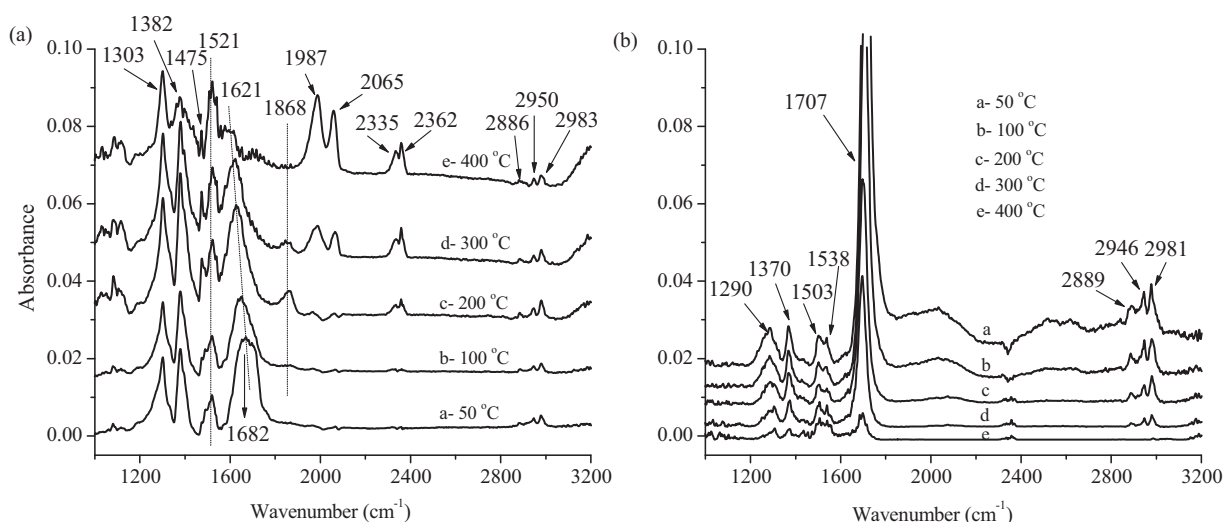


Fig. 4. The DRIFTS corresponding to propanoic acid adsorption over the 1.0Ru/ZrO₂ (a) and 1.0Ru/Al₂O₃ (b) catalysts in the absence of H₂ with TPD (50–400 °C).

catalysts surface become thermal unstable, and yet the decomposition of propionate and propanoyl species to CO/CO₂ is not occurred. These indicate that the surface species may be hydrogenated to propanol, although it is not confirmed by the DRIFTS. From these results, the C–C bond cleavage via the decarbonylation of propanoyl species or the decomposition of propionate species is significantly inhibited on the Ru/Al₂O₃ catalyst, and the formation of CO/CO₂ from the propanoyl or propionate species is greatly facilitated on the Ru/ZrO₂ catalyst surface.

To understand the surface reaction of intermediates in the presence of H₂, the in situ DRIFTS spectra for propanoic acid adsorbed on the samples were performed under vacuum at 180 °C, followed by introducing H₂ at different temperature. In the case of the Ru/ZrO₂ catalyst (Fig. 5), the spectra of adsorbed propionate (1483 and 1521 cm⁻¹) [55,56] and the analogous $\delta_s(-CH_3)$ and $\delta_{as}(-CH_3)$ stretching (1307 and 1400 cm⁻¹) [54–57] are observed. In addition, the C–H stretching in $\nu_{as}(-CH_3)$, $\nu_{as}(-CH_2)$ and $\nu_s(-CH_3)$ is not clearly observed in 2800–3000 cm⁻¹ region, and only very weak bands at both 2939 and 2983 cm⁻¹ are observed above 180 °C. The vanishing/weakening of C–H stretching region indicates that significant dissociation takes place [54]. As temperature increases, the spectrum shows two bands at 1949 and 2042 cm⁻¹ which are assigned to the adsorption of CO on Ru particles [49,60,61]. The appearance of adsorbed CO indicates the significant dissociation

and/or decarbonylation of propanoyl species on the Ru/ZrO₂ catalyst surface. At 200 and 210 °C, the band of adsorbed CH₄ appears at 3017 cm⁻¹ [62], which may be formed by methanation of the adsorbed CO on the Ru particles. Moreover, when the H₂ is firstly

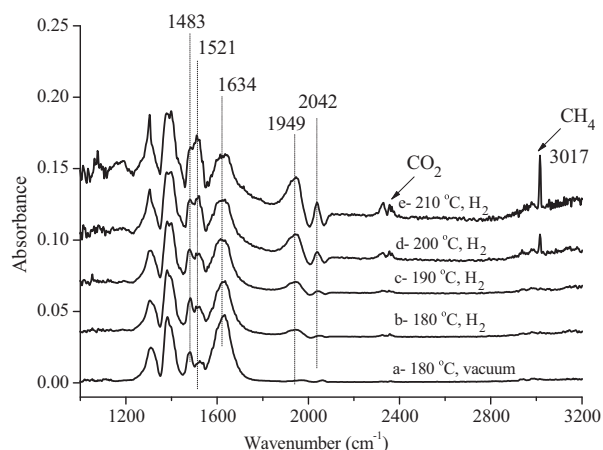


Fig. 5. The DRIFTS corresponding to propanoic acid adsorption over the 1.0Ru/ZrO₂ catalyst under flowing H₂ (180–210 °C).

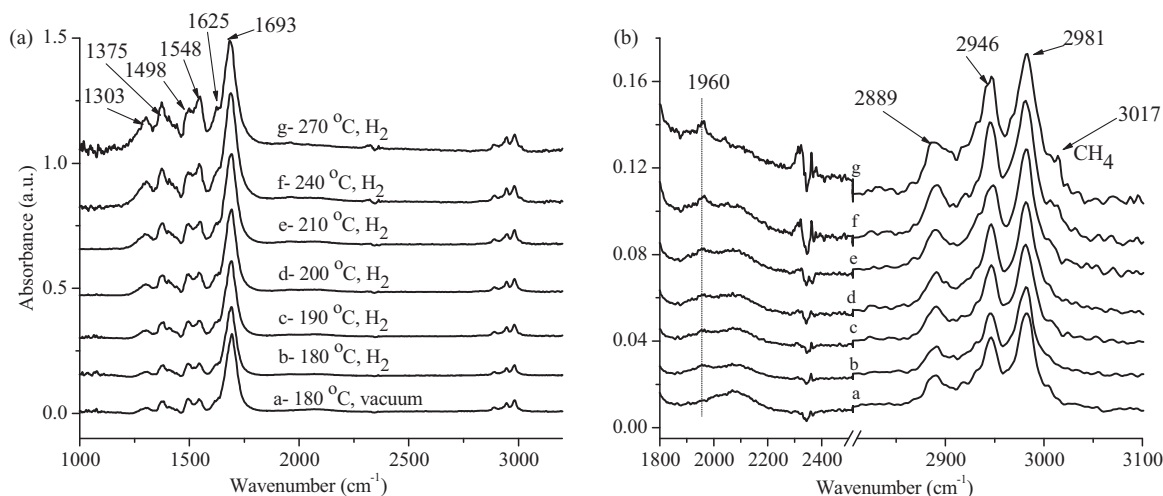


Fig. 6. The DRIFTS corresponding to propanoic acid adsorption over the 1.0Ru/Al₂O₃ catalyst under flowing H₂.

introduced at 180 °C, the adsorption of propanoyl (1634 cm⁻¹ band) [55,56,59] becomes weaker and the adsorption of CO on the surface becomes stronger. This phenomenon indicates that the presence of H₂ could favor the dissociation of propanoyl. In addition, the initial spectra of CO₂ clearly appear at 200 °C, while the spectra of CO clearly appear at the lower temperature (180 °C) than those of CO₂. These demonstrate that the presence of H₂ could favor the decarbonylation of propanoyl species other than decarboxylation of propionate species. Accordingly, we suggest that the adsorbed propanoic acid species over the Ru/ZrO₂ catalyst have a high selectivity towards C–C bond cleavage by decarbonylation of propanoyl species. In the presence of H₂, the methane can be formed by the methanation of CO adsorbed on the catalyst surface. The production of CO₂ may be due to the decomposition of propionate species or the oxidation of adsorbed CO at the higher temperature.

In the case of the Ru/Al₂O₃ catalyst, Fig. 6a shows a dominant band at 1693 cm⁻¹ and a very weak shoulder band at 1625 cm⁻¹, which may be ascribed to two different stretching modes of $\nu(-\text{CO})$ in propanoyl [55,56]. The spectra of adsorbed propionate (1498 and 1548 cm⁻¹) [55,56] and the analogous $\delta_s(-\text{CH}_3)$ and $\delta_{as}(-\text{CH}_3)$ stretching (1303 and 1375 cm⁻¹) [54–57] are also observed. Additionally, Fig. 6b shows no spectra of adsorbed CO and CH₄ are

detected below 210 °C, only very weak 1960 and 3017 cm⁻¹ bands are observed at 270 °C. Therefore, in the presence of H₂, the C–C bond cleavage by the decarbonylation of propanoyl species is also inhibited over the Ru/Al₂O₃ catalyst compared with the Ru/ZrO₂ catalyst.

3.3. Catalytic test

3.3.1. Hydrodeoxygenation of propanoic acid over the Ru/C catalyst

Fig. 7 shows the effects of temperature, pressure and WHSV on the catalytic activity and product selectivity for the APHDO of propanoic acid over the Ru/C catalyst. The products include propanol, alkanes (methane, ethane, and propane), and a trace amount of the degraded oxygenates (ethanol and acetic acid). Interestingly, nearly equimolar amounts of methane and ethane were produced. As shown in Fig. 7a, as the increase of temperature, the catalytic activity increased significantly (from 27.9 to 93.5% for conversion). The selectivity of propanol decreased sharply (from 45.8 to 2.7%), and the selectivity of C₁–C₃ alkanes increased greatly. Accordingly, the high temperature facilitates the conversion of propanoic acid to methane, ethane and propane via C–C or C–O cleavage, while low temperature

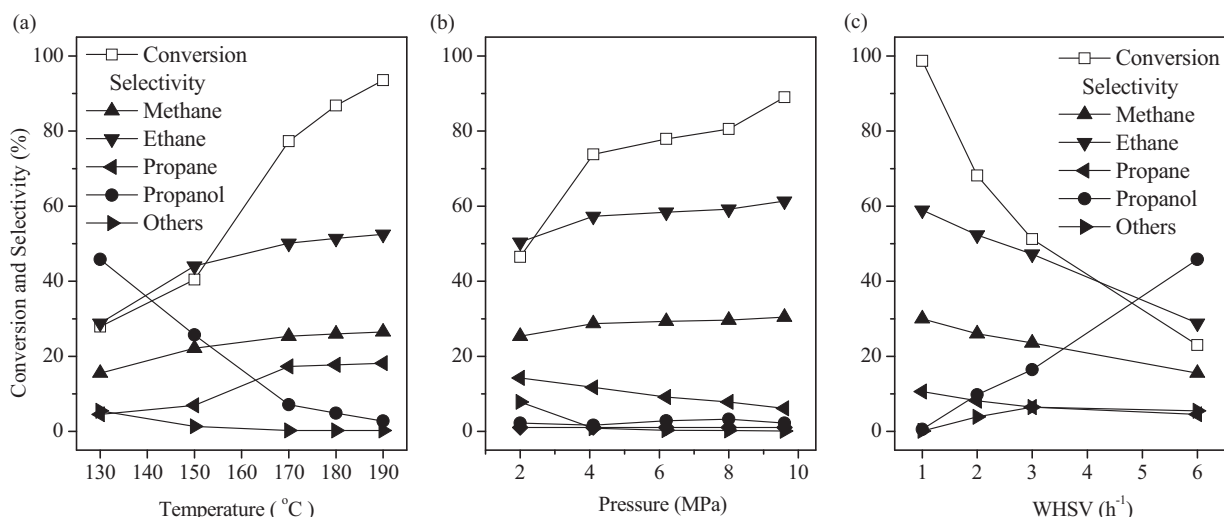


Fig. 7. The effects of temperature (a), pressure (b) and WHSV (c) on the conversion and product selectivity over the 1.0Ru/C catalyst.

Table 2
APHDO of the C₂–C₄ carboxylic acids over the 1.0Ru/C catalyst.^a

Reactant ^b	Temp. (°C)	Conv. (%)	Selectivity (%)					C ₁ /C _{n-1} ^e	
			Alcohol ^c	CH ₄	C ₂ H ₆	C ₃ H ₈	C ₄ H ₁₀		Others ^d
AA	150	23.3	71.1	22.2	1.2	–	–	5.5	–
	180	56.4	25.9	66.8	5.1	–	–	2.2	–
	190	76.9	6.9	76.3	16.7	–	–	0.1	–
PA	150	40.4	25.7	22.1	44.0	6.9	–	1.4	1.01
	180	86.8	4.8	25.9	51.4	17.7	–	0.2	1.01
	190	93.5	2.7	26.5	52.5	18.1	–	0.2	1.01
BA	190	93.5	3.3	22.3	0.2	64.4	9.6	0.3	1.04
IBA	190	85.4	7.0	21.1	0.1	62.5	9.1	0.2	1.02

^a Reaction conditions: 6.4 MPa, 1.0 h⁻¹, 80 cm³ min⁻¹ H₂ flow, and 0.83 M aqueous solution as feedstock.

^b AA, acetic acid; PA, propanoic acid; BA, butyric acid; IBA, isobutyric acid.

^c Alcohol with the same carbon atom as the substrate.

^d Others: the degraded oxygenates ethanol and acetic acid.

^e The molar ratio of methane and alkanes with one carbon atom less than the substrate.

favors the formation of propanol via C=O hydrogenation of carboxyl.

As shown in Fig. 7b, the conversion of propanoic acid increased from 46.5 to 89% significantly with the total pressure of the system increasing from 2.0 to 9.6 MPa. The selectivities of methane, ethane and propanol increased slightly, especially for propanol with a very small increase (1.6–3.2%), and the selectivity of propane decreased from 14.2 to 6.1%. Therefore, the C–C bond cleavage reaction is predominant at the high temperature (200 °C), and the hydrogen pressure has a little effect on the product selectivity but improves the catalytic activity greatly.

Fig. 7c displays that the selectivity of propanol increased from 0.1 to 44.9%, while the selectivity of C₁–C₃ alkanes decreased from 99.9 to 52.3%, as the conversion of propanoic acid decreased with the WHSV in the range of 1.0–6.0 h⁻¹. This indicates the increase of WHSV can improve the production of propanol with the decrease of the selectivity of C₁–C₃ alkanes.

3.3.2. Hydrodeoxygenation of carboxylic acids (C₂–C₄) over the Ru/C catalyst

The APHDO of several carboxylic acids (C₂–C₄) over the Ru/C catalyst, including acetic acid, propanoic acid, butyric acid and isobutyric acid, was also investigated. As shown in Table 2, the main products include methane, alcohol and alkane with corresponding carbon atom to the substrate (C_n-alcohol and C_n-alkane), and alkane with one carbon atom less than the substrate (C_{n-1}-alkane). At the high temperature (above 180 °C), the alkanes are predominant products. It is certain that the monocarboxylic acids have the

common hydrodeoxygenation performance over the supported Ru catalysts, i.e., the hydrogenation of carboxyl to alcohol, the cleavage of C–O bond to corresponding alkane, and the formation of equimolar quantities of methane and C_{n-1}-alkane via the cleavage of C–C bond adjacent to the oxygen atom.

In summary, the C=O hydrogenation of carboxyl and C–C bond cleavage routes is strongly affected by the reaction conditions for the APHDO of carboxylic acids. However, the catalysis of the supported Ru catalysts is strongly dependent on the nature of supports [34].

3.3.3. Hydrodeoxygenation of propanoic acid over Ru/ZrO₂ and Ru/Al₂O₃ catalysts

As shown in Table 3, the conversion of propanoic acid increased significantly from 35.2 to 96.0% with increasing the temperature from 170 to 210 °C over the Ru/ZrO₂ catalyst. The selectivity of propanol decreased sharply from 43.2 to 3.6%, and the selectivity of C₁–C₃ alkanes increased correspondingly. However, the conversion of propanoic acid increased mildly from 17.1 to 61.8% over the Ru/Al₂O₃ catalyst, the selectivity of propanol decreased slightly from 87.7 to 67.9% and the selectivity of C₁–C₃ alkanes exhibited no significant increase. Obviously, the high temperature favors the cleavage of C–C and C–O bonds (production of C₁–C₃ alkanes), while the Ru/Al₂O₃ catalyst has a lower selectivity of C₁–C₃ alkanes and a high selectivity of propanol. Nevertheless, the conversion of propanoic acid over the Ru/Al₂O₃ catalyst is lower than that of Ru/C and Ru/ZrO₂ catalysts under the same conditions. In high pressure aqueous environment, generally, the changes of support

Table 3
The effect of temperature on the conversion and product selectivity over the Ru/ZrO₂ and Ru/Al₂O₃ catalysts.^a

Catalyst	Temp. (°C)	Conv. (%)	Selectivity (%)					CH ₄ /C ₂ H ₆ ^c molar ratio
			Propanol	CH ₄	C ₂ H ₆	C ₃ H ₈	Others ^b	
1.0Ru/ZrO ₂	170	35.2	49.5	15.5	30.8	2.5	1.7	1.01
	180	47.0	43.2	17.2	34.3	3.2	2.1	1.00
	190	72.1	24.9	20.1	40.2	7.5	7.3	1.00
	200	93.6	4.5	28.1	56.1	10.4	0.9	1.00
	210	96.0	3.6	28.4	56.7	10.4	0.9	1.00
1.0Ru/Al ₂ O ₃	170	17.1	87.4	0.6	1.3	3.9	6.8	0.92
	180	35.0	87.7	1.2	2.5	4.9	3.6	0.96
	190	47.9	85.1	2.1	4.2	5.2	3.4	1.00
	200	58.3	68.3	5.9	11.7	13.7	0.5	1.01
	210	61.8	67.9	7.7	14.2	9.7	0.5	1.08

^a Reaction conditions: 6.4 MPa, 1.0 h⁻¹, 80 cm³ min⁻¹ H₂ flow, and 0.83 M propanoic acid as feedstock.

^b Others: the degraded oxygenates ethanol and acetic acid.

^c The molar ratio of methane and ethane.

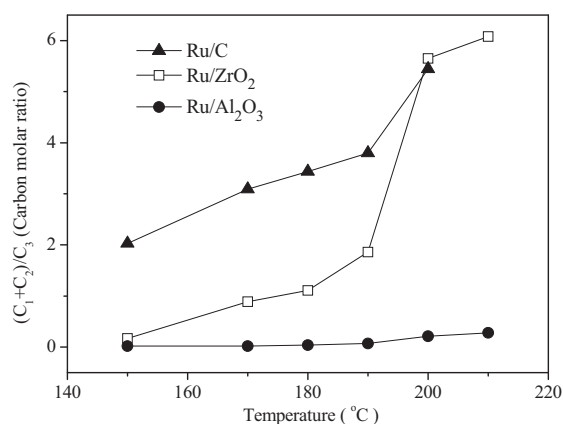


Fig. 8. The effect of temperature on the C–C bond cleavage or C=O hydrogenation over the Ru/C, Ru/ZrO₂ and Ru/Al₂O₃ catalysts.

Table 4
The selectivities of C=O hydrogenation and C–C bond cleavage products over the Ru/C, Ru/ZrO₂ and Ru/Al₂O₃ catalysts under similar conversions.

Catalyst	Conversion (%)	Selectivity (%)	
		Propanol and propane	Methane and ethane
1.0Ru/C	40.4	32.6	66.1
1.0Ru/ZrO ₂	35.2	52	46.3
1.0Ru/Al ₂ O ₃	35.0	92.6	3.7
1.0Ru/C	51.2	22.8	70.7
1.0Ru/ZrO ₂	47.0	46.4	51.5
1.0Ru/Al ₂ O ₃	47.9	90.3	6.3

structure during reaction could induce the decrease of catalytic activity [63]. The Ru/Al₂O₃ catalyst exhibiting the lowest conversion of propanoic acid is likely ascribed to the structural unstable of γ -alumina in aqueous environment [63]. In addition, the low conversion of Ru/Al₂O₃ may be attributed to the low Ru dispersion (Table 1). In this work, we focus mainly on the difference of reaction routes (C=O hydrogenation, C–C bond cleavage) over the Ru/C, Ru/ZrO₂ and Ru/Al₂O₃ catalysts.

Fig. 8 shows the behavior of C–C bond cleavage/C=O hydrogenation as a function of temperature over the Ru/C, Ru/ZrO₂ and Ru/Al₂O₃ catalysts. The cleavage of C–C bond to produce methane and ethane is greatly inhibited over the Ru/Al₂O₃ catalyst. Specifically, as the temperature increases, the (CH₄ + C₂H₆)/(C₃H₈ + C₃H₇OH) molar ratio obtained from the Ru/Al₂O₃ catalyst increases much less than that of the Ru/ZrO₂ and Ru/C catalysts. As given in Table 4, under similar conversions of 35–40%, about 92.6% selectivity for C₃-products (propanol and propane) are obtained over the Ru/Al₂O₃ catalyst, while only 52% and 32.6% are obtained over the Ru/ZrO₂ and Ru/C catalysts, respectively. The selectivity of C–C bond cleavage products (methane

Table 5
The selectivities of C=O hydrogenation and C–C bond cleavage products over the Ru/ZrO₂ and Ru/Al₂O₃ catalysts with different Ru loading.^a

Catalyst	Temperature (°C)	WHSV (h ⁻¹)	Conversion (%)	Selectivity (%)	
				Propanol and propane	Methane and ethane
1.0Ru/ZrO ₂	190	3.0	43.3	52.4	44.1
4.0Ru/ZrO ₂	190	6.0	41.8	48.3	44.4
6.0Ru/ZrO ₂	190	6.0	50.5	42.4	55.9
1.0Ru/Al ₂ O ₃	200	3.0	32.8	90.3	8.9
4.0Ru/Al ₂ O ₃	200	8.0	37.1	82.7	10.5
6.0Ru/Al ₂ O ₃	200	9.0	34.9	73.6	16.6

^a Reaction conditions: 6.4 MPa, 120 cm³ min⁻¹ H₂ flow, and 0.83 M propanoic acid as feedstock.

and ethane) for the Ru/ZrO₂ (46.3%) and Ru/C (66.1%) catalysts are apparently higher than that of the Ru/Al₂O₃ catalyst (3.7%). Under the similar conversions of 47–52%, the selectivity of C₃-products (90.3%) for the Ru/Al₂O₃ catalyst is approximately double of Ru/ZrO₂ catalyst (46.4%) and is about four times of Ru/C catalyst (22.8%). Correspondingly, the selectivity of C–C bond cleavage products (6.3%) is greatly lower than that of the Ru/ZrO₂ (51.5%) and Ru/C (70.7) catalysts. It is concluded that the production of propanol and propane by the C=O hydrogenation of propanoic acid is improved over the Ru/Al₂O₃ catalyst where the cleavage of C–C bond to methane and ethane is greatly inhibited. However, the cleavage of C–C bond is greatly enhanced over the Ru/ZrO₂ and Ru/C catalysts. These results are also confirmed by the DRIFTS results of propanoic acid (Figs. 4–6).

In addition, the contribution of metal should be considered in the APHDO reaction in order to selectively produce higher or lower alkanes, since C–C bond cleavage generally occurs on metal sites. As shown in Table 5, under similar conversions, the products of C–C bond cleavage increase from 44.1 to 55.9% with the increase of Ru metal loading for Ru/ZrO₂ catalyst. The same trend is observed over the Ru/Al₂O₃ catalyst (from 8.9 to 16.6%), but it is much lower than that of Ru/ZrO₂ catalyst. Consequently, the higher amounts of Ru will lead to a favorable formation of CH₄ and C₂H₆ from propanoic acid. Although the high Ru contents favors the formation of methane and ethane from propanoic acid, the Al₂O₃ support in combination with Ru metal still can favor the C=O hydrogenation of carboxyl compared with that of ZrO₂ support. For the Ru/Al₂O₃ catalyst with high Ru contents, the selectivity of C=O hydrogenation products is still much higher than C–C bond cleavage products. It is indicated that the C=O hydrogenation and C–C bond cleavage are mainly dependent on the nature of support. However, the contribution of Ru metal should be also considered. Therefore, the balancing each contribution of metal and support is crucial in the APHDO reaction in order to selectively produce desired production.

3.3.4. Hydrodeoxygenation of carboxylic acid in the absence of H₂

We performed another test to investigate the formation of CO/CO₂ and their methanation in aqueous-phase system. The catalytic test was carried out over the Ru/ZrO₂ catalyst at 200 °C, 6.4 MPa, 3.0 h⁻¹, 80 cm³ min⁻¹ H₂ or N₂ flow, and 0.83 M propanoic acid as feedstock. After catalyst was reduced in a H₂ flow, the H₂ was purged out and the reaction pressure was adjusted by N₂. After running 60 h, the N₂ flow was switched to H₂ flow.

As shown in Fig. 9, before switching to H₂ flow, the low propanoic acid conversion (ca. 30%) is observed. The concentrations of CO₂ and CH₄ in the effluent gas are 0.9 and 0.5%, respectively. However, the CO is still not detected in the effluent gas. In fact, the CO and water can be transformed to CO₂ and H₂ by water gas shift (WGS), and the methanation of CO and/or CO₂ can give the CH₄ [64]. The extremely low levels of CO compared to the amounts of CO₂ and CH₄ could be ascribed to the high WGS activity and high methanation activity of CO on the Ru catalyst [64]. Under similar

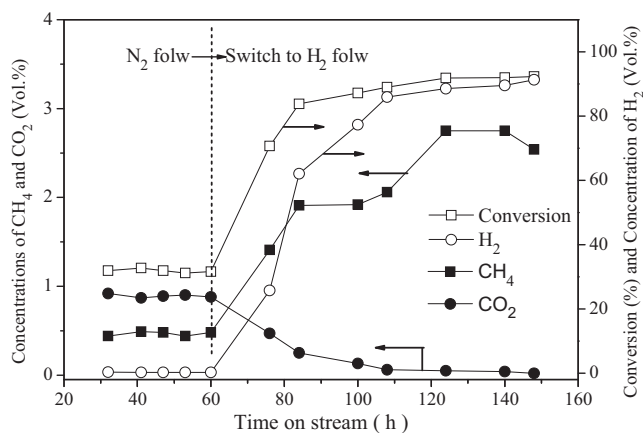


Fig. 9. APHDO of propanoic acid over the 1.0Ru/ZrO₂ catalyst in a continue H₂-N₂-H₂ stream.

conditions, Davda et al. [64] reported that the relatively low levels of CO were produced compared to the amount of CO₂ formed from the aqueous-phase reforming of ethylene glycol, e.g., ethylene glycol reforming over the supported Ru catalyst resulted in CO/CO₂ ratios of 0.05, even lower amounts of CO were produced over Pt and Rh, with CO/CO₂ ratios lower than 0.004. Therefore, it is accepted that the CO is not detected in our experiments due to its concentration is below the detection limit of GC.

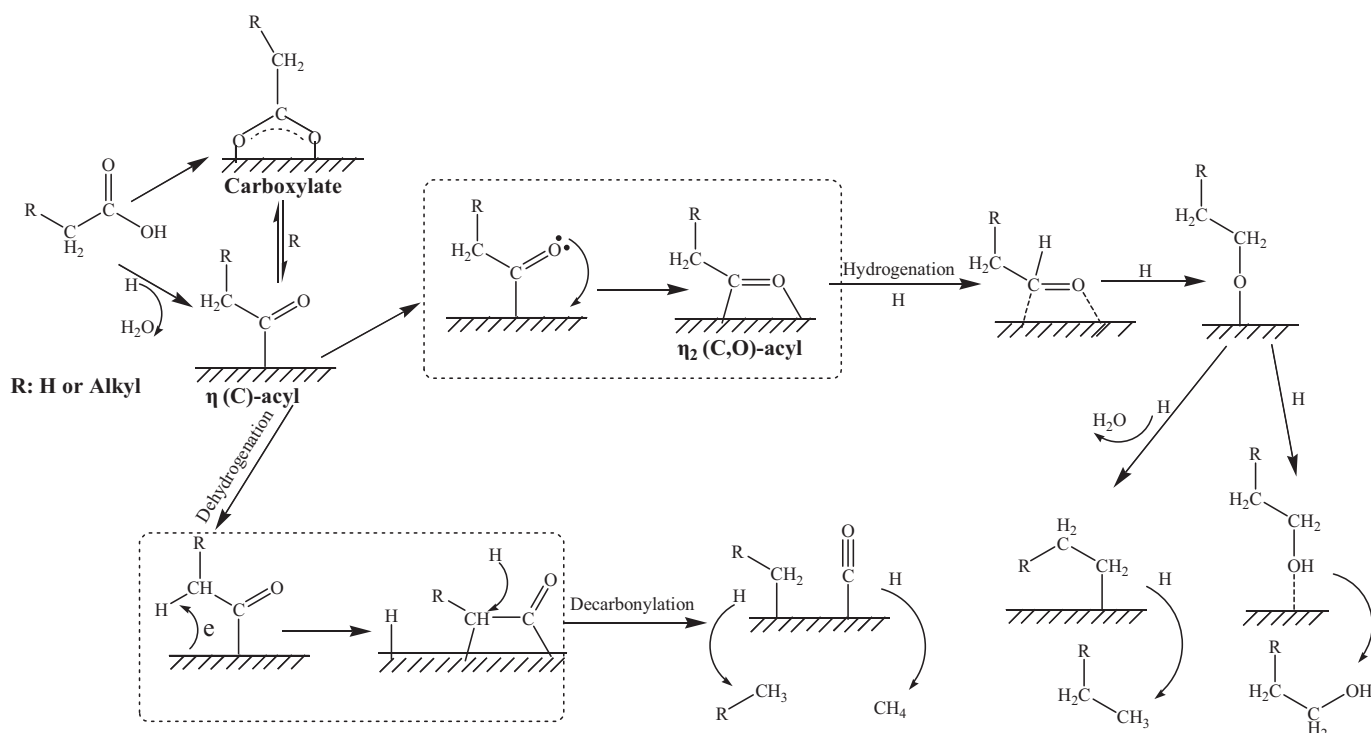
When the N₂ flow was substituted with H₂, the concentration of H₂ in the effluent gas increased from 0.24 to 91% on the time stream, and the conversion of propanoic acid increased greatly from 31 to 99%. At the same time, the concentration of CH₄ in the effluent gas increased from 0.5% to the maximum value of 2.8%, while the concentration of CO₂ decreased from 0.9 to 0.02% and the CO was still not detected. It is sure that the catalytic activity can be significantly improved by increasing H₂ partial pressure. In this reaction system, the concentration of CO₂ became less and less (0.02%) with

the increase of H₂ partial pressure, as well as, no CO was observed in the effluent gas all along, indicating that the nearly completed methanation of CO or CO₂ was possible for the APHDO of propanoic acid over the supported Ru catalysts.

3.4. APHDO mechanism of carboxylic acids

The detail reaction mechanisms, for conversion of acetic acid to ethanol, have been studied over transition metal catalysts by combined experimental and DFT calculations theoretical study [17,65]. In the postulated mechanism, acetic acid dissociates to form an acetyl surface species directly or via acetate intermediate. The acetyl intermediate is then subsequently hydrogenated to ethanol via the formation of an acetaldehyde surface intermediate. In addition, Mavrikakis and Barteau reviewed the decomposition mechanisms of oxygenates on transition metal surfaces [66]. They concluded that decarbonylation of aldehydes and alcohols over Group VIII metals to produce CO via the formation of acyl intermediates on metal surfaces [57,66,67]. The formation of acetyl is the likely precursor to the formation of CO from C₂ oxygenates [57]. Indeed, several references have reported that the decomposition of C₂-oxygenates, such as acetic acid and acetaldehyde, to CO is preceded by the formation of surface-bound acetyl intermediate [57,67–70]. It is suggested that the β C–H bond activation of the methyl group on acetyl or acetate to produce ketene intermediate (CH₂CO), is rate determining for CO/CO₂ and methyl surface fragments production with C–C scission of ketene. Henderson et al. have also proposed that the adsorbed ketene (CH₂CO) as η²(C, C) on the Ru crystals may dissociate to CO and methylene [71,72].

In this study, the C₃-products (propanol and propane) as well as the equimolar amounts of methane and C_{n-1}-alkane were observed in the all APHDO tests of carboxylic acids. The DRIFTS spectra of propanoic acid adsorbed on the Ru/ZrO₂ catalyst surface (Figs. 4 and 5) showed that the CO was formed by the decarbonylation of propanoyl species by changing of its configuration with the increase of temperature, and then it was hydrogenated



Scheme 1. The surface reaction model of C=O hydrogenation and C–C bond cleavage for carboxylic acid hydrodeoxygenation over the supported Ru catalysts.

to methane in the presence of H₂ at high temperature. Accordingly, we think that the acyl is a key intermediate for the C=O hydrogenation and C–C bond cleavage of carboxylic acid functional group. The hydrodeoxygenation mechanism of carboxylic acid over the supported Ru catalyst is proposed in Scheme 1. The carboxylic acid molecule dissociates to form the acyl surface species directly or via carboxylate intermediate over Ru metal firstly. Consequently, one pathway is that the acyl intermediate is catalyzed by Ru metal to produce adsorbed CO plus hydrocarbon moieties after the β C–H bond activation of the acyl. Finally, the methane and C_{n-1}-alkane are produced by hydrogenation of adsorbed CO and hydrocarbon moieties on Ru metal. Another pathway is that the acyl intermediate is hydrogenated to alcohol via formation of aldehyde intermediate. In addition, a fast equilibrium reaction may be existed between the acyl species and the adsorbed alcohol/aldehyde species. This equilibrium reaction will lead to the C–C bond cleavage of the alcohol/aldehyde. Furthermore, the produced alcohol from carboxylic acid can be further hydrogenated to corresponding alkane. This was reported for alcohols converted into corresponding alkane via dehydration-hydrogenation over the acid/metal bifunctional catalysts [8,11,22].

3.5. Effect of support on reaction of C–C bond cleavage

The reaction kinetics data and DRIFTS characterization results reveal that the C–C bond cleavage via decarbonylation of the acyl is greatly inhibited over the Ru/Al₂O₃ catalyst compared to the Ru/ZrO₂ (or Ru/C) catalyst. The inhibition ability of C–C bond cleavage increases in the follow order: Ru/C < Ru/ZrO₂ < Ru/Al₂O₃. Based on the characterizations of catalysts (H₂-TPR, NH₃-TPD, CO-FTIR), the metal–support interaction and surface acidity of catalysts increases in the following order: Ru/C < Ru/ZrO₂ < Ru/Al₂O₃. In addition, the CO-FTIR reveals that the electronic state of Ru species on the Ru/Al₂O₃ catalyst is electron deficient compared with those of Ru/ZrO₂ catalyst. Therefore, it is possible that the effect of support on the reaction route for APHDO of carboxylic acids is attributed to these factors of catalyst, i.e., surface acidity, metal–support interaction and electronic state of Ru species. The stronger metal–support interaction and electronic state of Ru species. The stronger metal–support interaction, the more electron deficient ruthenium species (Ru⁴⁺) and the more acidity sites on the catalyst will lead to the higher extent of C=O hydrogenation or lower extent of C–C bond cleavage.

4. Conclusions

For carboxylic acid APHDO over the Ru/C, Ru/ZrO₂ and Ru/Al₂O₃ catalysts, the high temperature, as well as, the catalysts with high Ru loading facilitated the cleavage of C–C bond, while acidic support in combination with a metal favored the hydrogenation of carboxyl. The DRIFTS results revealed that the C–C bond cleavage was induced by the decarbonylation of acyl on the catalyst. The C–C bond cleavage was favored in the order of Ru/C > Ru/ZrO₂ > Ru/Al₂O₃. Based on H₂-TPR, NH₃-TPD and CO-FTIR, the effect of support on the reaction routes may be attributed to surface acidity, electronic state of Ru species and metal–support interaction of catalyst.

Acknowledgements

The authors gratefully thank the financial supports of Major State Basic Research Development Program of China (973 Program) (No. 2012CB215305) and Natural Science Foundation of China (No. 20976185). We also thank Dr. Guoqiang Ding for valuable discussion during manuscript preparation.

References

- [1] C.H. Christensen, J. Rass-Hansen, C.C. Marsden, E. Taarning, K. Egeblad, *ChemSusChem* 1 (2008) 283–289.
- [2] J.H. Clark, F.E.I. Deswarte, T.J. Farmer, *Biofuels Bioprod. Bioref.* 3 (2009) 72–90.
- [3] Y.C. Lin, G.W. Huber, *Energy Environ. Sci.* 2 (2009) 68–80.
- [4] G. Centi, R.A. van Santen (Eds.), *Catalysis for Renewables*, Wiley-VCH, Weinheim, Germany, 2007, p. 53.
- [5] J.J. Bozell, G.R. Petersen, *Green Chem.* 12 (2010) 539–554.
- [6] Z.G. Zhang, J.E. Jackson, D.J. Miller, *Appl. Catal. A* 219 (2001) 89–98.
- [7] Z.G. Zhang, J.E. Jackson, D.J. Miller, *Ind. Eng. Chem. Res.* 41 (2002) 691–696.
- [8] J.N. Chheda, J.A. Dumesic, *Catal. Today* 123 (2007) 59–70.
- [9] J.C. Serrano-Ruiz, J.A. Dumesic, *Green Chem.* 11 (2009) 1101–1104.
- [10] J.C. Serrano-Ruiz, J.A. Dumesic, *ChemSusChem* 2 (2009) 581–586.
- [11] R.M. West, M.H. Tucker, D.J. Braden, J.A. Dumesic, *Catal. Commun.* 10 (2009) 1743–1746.
- [12] Z.G. Zhang, J.E. Jackson, D.J. Miller, *Bioresour. Technol.* 99 (2008) 5873–5880.
- [13] Y.Q. Chen, D.J. Miller, J.E. Jackson, *Ind. Eng. Chem. Res.* 46 (2007) 3334–3340.
- [14] C. Delhomme, D. Weuster-Botz, F.E. Kühn, *Green Chem.* 11 (2009) 13–26.
- [15] J.N. Chheda, Y. Román-Leshkov, J.A. Dumesic, *Green Chem.* 9 (2007) 342–350.
- [16] J.C. Serrano-Ruiz, D. Wang, J.A. Dumesic, *Green Chem.* 12 (2010) 574–577.
- [17] H. Olcay, L. Xu, Y. Xu, G.W. Huber, *ChemCatChem* 2 (2010) 1420–1424.
- [18] N. Li, G.W. Huber, *J. Catal.* 270 (2010) 48–59.
- [19] A. Wawrzetz, B. Peng, A. Hrabar, A. Jentys, A.A. Lemonidou, J.A. Lercher, *J. Catal.* 269 (2010) 411–420.
- [20] G.W. Huber, J.N. Chheda, C.J. Barrett, J.A. Dumesic, *Science* 308 (2005) 1446–1450.
- [21] J.C. Serrano-Ruiz, J.A. Dumesic, *Energy Environ. Sci.* 4 (2011) 83–99.
- [22] G.W. Huber, J.A. Dumesic, *Catal. Today* 111 (2006) 119–132.
- [23] F.T. Jere, D.J. Miller, J.E. Jackson, *Org. Lett.* 5 (2003) 527–530.
- [24] G.W. Huber, J.A. Dumesic, *Angew. Chem. Int. Ed.* 43 (2004) 1549–1551.
- [25] G.W. Huber, P. O'Connor, A. Corma, *Appl. Catal. A* 329 (2007) 120–129.
- [26] J.N. Chheda, G.W. Huber, J.A. Dumesic, *Angew. Chem. Int. Ed.* 46 (2007) 7164–7183.
- [27] T.P. Vispute, G.W. Huber, *Green Chem.* 11 (2009) 1433–1445.
- [28] G.W. Huber, S. Iborra, A. Corma, *Chem. Rev.* 106 (2006) 4044–4098.
- [29] A. Corma, S. Iborra, A. Velty, *Chem. Rev.* 107 (2007) 2411–2502.
- [30] R. Luque, J.H. Clark, K. Yoshida, P.L. Gai, *Chem. Commun.* (2009) 5305–5307.
- [31] R. Luque, J.H. Clark, *Catal. Commun.* 11 (2010) 928–931.
- [32] T. Miyazawa, S. Koso, K. Kunimori, K. Tomishige, *Appl. Catal. A* 329 (2007) 30–35.
- [33] E.P. Maris, R.J. Davis, *J. Catal.* 249 (2007) 328–337.
- [34] E.S. Vasiliadou, E. Heracleous, I.A. Vasalos, A.A. Lemonidou, *Appl. Catal. B* 92 (2009) 90–99.
- [35] T. Miyazawa, Y. Kusunoki, K. Kunimori, K. Tomishige, *J. Catal.* 240 (2006) 213–221.
- [36] H. Kobayashi, T. Komanoya, K. Hara, A. Fukuoka, *ChemSusChem* 3 (2010) 440–443.
- [37] J.H. Zhou, M.G. Zhang, L. Zhao, P. Li, X.G. Zhou, W.K. Yuan, *Catal. Today* 147 (2009) S225–S229.
- [38] M. Kantcheva, S. Sayan, *Catal. Lett.* 60 (1999) 27–38.
- [39] S. Hosokawa, H. Kanai, K. Utani, Y. Taniguchi, Y. Saito, S. Imamura, *Appl. Catal. B* 45 (2003) 181–187.
- [40] R. Lanza, S.G. Järäs, P. Canu, *Appl. Catal. A* 325 (2007) 57–67.
- [41] P. Betancourt, A. Rives, R. Hubaut, C.E. Scott, J. Goldwasser, *Appl. Catal. A* 170 (1998) 307–314.
- [42] I. Rossetti, N. Pernicone, L. Forni, *Appl. Catal. A* 248 (2003) 97–103.
- [43] J.L. Bi, Y.Y. Hong, C.C. Lee, C.T. Yeh, C.B. Wang, *Catal. Today* 129 (2007) 322–329.
- [44] H. Ishikawa, J.N. Kondo, K. Domen, *J. Phys. Chem. B* 103 (1999) 3229–3234.
- [45] M.G. Cattania, F. Parmigiani, V. Ragaini, *Surf. Sci.* 211/212 (1989) 1097–1105.
- [46] K. Asakura, Y. Iwasawa, *J. Chem. Soc. Faraday Trans.* 86 (1990) 2657–2662.
- [47] M.W. McQuire, C.H. Rochester, *J. Catal.* 157 (1995) 396–402.
- [48] G.H. Yokomizo, C. Louis, A.T. Bell, *J. Catal.* 120 (1989) 1–14.
- [49] S.Y. Chin, C.T. Williams, M.D. Amiridis, *J. Phys. Chem. B* 110 (2006) 871–882.
- [50] B.A. Riguette, J.M.C. Bueno, L. Petrov, C.M.P. Marques, *Spectrochim. Acta Part A: Mol. Biomol. Spectrosc.* 59 (2003) 2141–2150.
- [51] C. Elmasides, D.I. Kondarides, W. Grünert, X.E. Verykios, *J. Phys. Chem. B* 103 (1999) 5227–5239.
- [52] V. Mazzieri, F. Coloma-Pascual, A. Arcoya, P.C. L'Argentière, N.S. F'goli, *Appl. Surf. Sci.* 210 (2003) 222–230.
- [53] T. Mitsui, K. Tsutsui, T. Matsui, R. Kikuchi, K. Eguchi, *Appl. Catal. B* 81 (2008) 56–63.
- [54] A.R. Garcia, J.L. da Silva, L.M. Ilharco, *Surf. Sci.* 415 (1998) 183–193.
- [55] W. Rachmady, M.A. Vannice, *J. Catal.* 207 (2002) 317–330.
- [56] M.K. Gnanamani, G. Jacobs, R.A. Keogh, B.H. Davis, *J. Catal.* 277 (2010) 27–35.
- [57] J.L. Davis, M.A. Barteau, *Surf. Sci.* 235 (1990) 235–248.
- [58] A. Yee, S.J. Morrison, H. Idriss, *J. Catal.* 191 (2000) 30–45.
- [59] M. Heinen, Z. Jusys, R.J. Behm, *J. Phys. Chem. C* 114 (2010) 9850–9864.

- [60] D. Gottschalk, E.A. Hinson, A.S. Baird, H.L. Kitts, K.A. Layman, J. Phys. Chem. C 114 (2010) 4950–4960.
- [61] R.L. Martins, M.A.S. Baldanza, M. Schmal, J. Phys. Chem. B 105 (2001) 10303–10307.
- [62] G. Busca, T. Montanari, C. Resini, G. Ramis, U. Costantino, Catal. Today 143 (2009) 2–8.
- [63] W.C. Ketchie, E.P. Maris, R.J. Davis, Chem. Mater. 19 (2007) 3406–3411.
- [64] R.R. Davda, J.W. Shabaker, G.W. Huber, R.D. Cortright, J.A. Dumesic, Appl. Catal. B 43 (2003) 13–26.
- [65] V. Pallassana, M. Neurock, J. Catal. 209 (2002) 289–305.
- [66] M. Mavrikakis, M.A. Barteau, J. Mol. Catal. A: Chem. 131 (1998) 135–147.
- [67] R. Shekhar, M.A. Barteau, R.V. Plank, J.M. Vohs, J. Phys. Chem. B 101 (1997) 7939–7951.
- [68] J.L. Davis, M.A. Barteau, J. Am. Chem. Soc. 111 (1989) 1782–1792.
- [69] J.L. Davis, M.A. Barteau, Surf. Sci. 256 (1991) 50–66.
- [70] R. Shekhar, M.A. Barteau, Catal. Lett. 31 (1995) 221–237.
- [71] M.A. Henderson, P.L. Radloff, C.M. Greenlief, J.M. White, C.A. Mims, J. Phys. Chem. 92 (1988) 4120–4127.
- [72] M.A. Henderson, P.L. Radloff, J.M. White, C.A. Mims, J. Phys. Chem. 92 (1988) 4111–4119.